

Evolution of Growth Modes for Polyelectrolyte Bundles

Ghee Hwee Lai,¹ Rob Coridan,¹ Olena V. Zribi,¹ Ramin Golestanian,² and Gerard C. L. Wong^{1,3,*}

¹*Department of Physics, University of Illinois at Urbana-Champaign, Urbana-Champaign, Illinois 61801, USA*

²*Department of Physics and Astronomy, University of Sheffield, Sheffield S3 7RH, United Kingdom*

³*Department of Materials Science & Engineering, University of Illinois at Urbana-Champaign, Illinois 61801, USA*

(Received 17 October 2006; published 30 April 2007)

Multivalent ions induce attractions between polyelectrolytes, but lead to finite-sized bundles rather than macroscopic phase separation. The kinetics of aggregation and bundle formation of actin is tracked using two different fluorescently labeled populations of *F*-actin. It is found that the growth mode of these bundles evolves with time and salt concentration, varying from an initial lateral growth to a longitudinal one at later stages. The results suggest that kinetics play a role in bundle growth, but not in the lateral size of bundles, which is constant for linear and branched topologies.

DOI: [10.1103/PhysRevLett.98.187802](https://doi.org/10.1103/PhysRevLett.98.187802)

PACS numbers: 61.25.Hq, 64.75.+g, 82.35.Pq

Correlations between multivalent ions can induce the formation of close-packed bundles of like-charged polyelectrolytes [1]. Such polyelectrolyte aggregation has been observed for different biopolymers [2–6], and is relevant to a wide range of problems, such as DNA packaging [3,7], cytoskeletal regulation [8], and cystic fibrosis [9]. While different polyelectrolytes require different valencies and concentrations of counterions to induce bundle formation [5,6,10], there is a generic feature in these experiments: the bundles are always of finite size.

The observation of finite-sized bundles is puzzling, since theoretical descriptions of polyelectrolyte condensation predict infinitely large aggregates in equilibrium and macroscopic phase separation [11]. To resolve this, it has been suggested that kinetics play a role. In solution, most rods meet at an angle with a repulsive interaction, thus slowing down the growth kinetics and resulting in metastable bundles of finite size [12]. Alternatively, finite-sized equilibrium bundles may occur if steric effects in the packing of counterions prevent neutralization of the bundle [13], or if inherent frustration of the bundle structure exacts an energy penalty [4,13]. Computer simulations of bundle formation also indicate the tendency towards a finite aggregate size [14–16].

In this Letter, we use confocal microscopy to investigate the time evolution of Mg^{2+} induced *F*-actin bundles. We track the growth of over 20 000 bundles using two fluorescently labeled populations of *F*-actin (red and green) to explore how filaments add to existing bundles, how filaments mix within a bundle, and how bundles interact with one another. The growth mode evolves with time, starting with initial rapid lateral growth to a saturation in bundle width, followed by subsequent longitudinal bundle growth. A range of saturation bundle widths is observed, most of which are <100 nm, which has been independently confirmed with electron microscopy (EM). The size range is insensitive to Mg^{2+} concentration (from just above the onset of bundle formation at ~ 25 mM [2,8] up to the reentrant dissolution limit of $\sim 1.1M$), and persists for linear and branched topologies, with the same observed

width for successive generations of branches. This is confirmed by EM images with single-filament resolution that show how a size-limited bundle evolves into two such bundles at a branch. Interestingly, late-stage bundle-bundle interactions, which are not yet accessible to computer simulations, vary with salt level. End-to-end longitudinal aggregation of bundles via junctions is the dominant growth mode at high salt. The temporal evolution of junction densities approximately follows Smoluchowski flocculation kinetics and the system essentially stops evolving after free filaments in solution are depleted. The results show that kinetics do play an important role in controlling the length of the bundles rather than the width, and in the internal mixing of filaments within bundles.

Monomeric actin (*G*-actin, m.w. 43 000) in a 2 mg/ml solution (5 mM Tris buffer at pH 8.0, with 0.2 mM $CaCl_2$, 0.5 mM ATP, 0.2 mM DTT, and 0.01% NaN_3) was polymerized into *F*-actin at 100 mM KCl for 1 h. *F*-actin was treated with human plasma gelsolin to control length and with phalloidin to prevent depolymerization. The *F*-actin was centrifuged at 100×10^3 g for an hour, resuspended in H_2O (0.03–0.1 mg/ml), and labeled with two different dyes: green (Alexa Fluor 488 C_5 -maleimide) and red (Alexa Fluor 546 C_5 -maleimide) at Cys-374 of actin. Unlike phalloidin dyes, these dyes bind covalently to *F*-actin and do not migrate.

A Leica SP2 confocal microscope (point spread function of 0.25 μm measured with 3.8 nm quantum dots) was used to image *F*-actin bundles, the widths of which were measured with an automated edge-finding program. Typically, more than 30 bundles were measured per image and more than 30 images were analyzed to obtain a single averaged measurement. EM was performed with a JEOL 2100 (Gatan $1k \times 1k$ CCD), and samples were negatively stained with pH 6.8 Nano-*W* (nanoprobes).

Time-lapse images at the onset of condensation [Fig. 1(a)] unambiguously show a rapid saturation in bundle width followed by bundle elongation [17,18]. Using confocal microscopy at optical resolution, we estimate the mean virtual bundle width to be $\sim 0.29 \mu m$ for

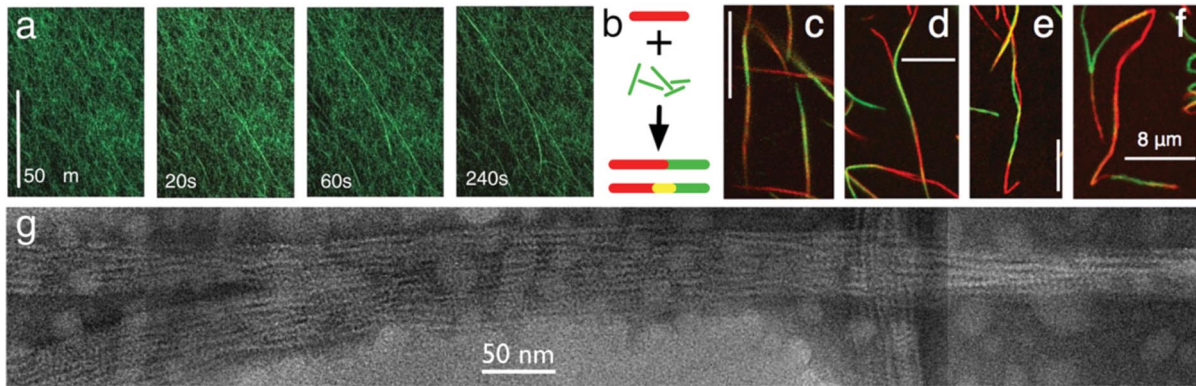


FIG. 1 (color). (a) Time-lapse sequence of actin bundle growth near onset of condensation shows dominant longitudinal growth mode. (b) Schematic of longitudinal growth between bundle and filaments. (c) Longitudinal growth as green “tracer” filaments add onto red bundles at 70 mM $[Mg^{2+}]$. (d)–(f) Longitudinal aggregation between red and green bundles at 50, 60, and 100 mM $[Mg^{2+}]$. Scale bar in (c)–(f) is 8 μm . (g) 5 negative stain (pH 7) TEM images stitched together to show a bundle junction, prepared at 30 mM $[Mg^{2+}]$.

the solution conditions examined here, although larger bundles at $\sim 0.40 \mu\text{m}$ exist. This average width is roughly constant for $[Mg^{2+}]$ from just above the onset of bundle formation at $\sim 25 \text{ mM}$ to the threshold of bundle dissolution at $\sim 1.1 \text{ M}$, above which bundles are observed to redissolve. It is also insensitive to actin concentration over the limited range studied (0.03 mg/ml–0.1 mg/ml). After deconvolving the instrumental point spread function, this implies a mean bundle width of $\sim 40 \text{ nm}$, with the largest observed bundles in the $\sim 100 \text{ nm}$ range. Smaller presaturation aggregates are observed at lower salt levels, but their size polydispersity and rapid time evolution prevent a reliable measurement using a scanning probe like confocal microscopy.

In order to evaluate potential sources of kinetic constraints, it is important to see how individual filaments are incorporated to existing bundles. We prepared bundles composed of red (Alexa 546) *F*-actin (0.03 mg/ml) at well-defined salt concentrations and added trace amounts [$\sim(5\text{--}10)\times$ smaller] of green (Alexa 488) *F*-actin to the solution with no added salt. We observed that the bundles grow longitudinally, keeping their width constant [see Fig. 1(c), where bundles of the same saturation width transition from one color to another]. An interesting feature in these bundles is the significant mixing of red and green filaments around junctions. The yellow junction regions correspond to the colocalization of red and green filaments [Fig. 1(b)].

The fact that many bundles exhibit more than two color transitions along their lengths suggests the occurrence of longitudinal bundle aggregation [19]. Examples of such longitudinal bundle aggregation can be seen in Figs. 1(d)–1(f), which show snapshots of mixing red bundles and green bundles at constant initial salt concentration. We find that bundles either remain unconnected or aggregate end-to-end [20]. The mean virtual bundle width is found to be $\sim 0.29 \mu\text{m}$ around junctions, the same as the previously measured saturation bundle width. Even for branched bun-

dles, we find uniform bundle widths before and after the junctions.

Using high resolution EM, we measure the range of bundle widths for the present solution conditions, and find $\sim(40\text{--}120) \text{ nm}$, in agreement with confocal microscopy estimates above. Figure 1(g) shows a negative stain image of a branched bundle. It can be seen clearly that although the junction itself is wider than the observed width limit, the bundle width well before and well after the junction returns to the same limited size, also in agreement with our low-resolution confocal microscopy results. This suggests that when a bundle locally grows beyond its size limit, it can split off into two bundles below the size limit.

Interestingly, the filaments on the surfaces of representative finite-sized bundles are disordered [Fig. 1(g)]. This disorder may play an important role in the mechanism of the size limit. In the large (\sim micron) actin bundles in the published literature [21], the actin is significantly more ordered, in contrast to our results with the small $\sim 100 \text{ nm}$ bundles. We hypothesize that different solution conditions potentially lead to different degrees of ordering within bundles, and result in different size limits.

To track the long-term evolution of junction formation, different time series of images were collected at different $[Mg^{2+}]$. *F*-actin–Mg samples (0.03 mg/ml) were allowed to bundle for 10 min before the mixing of red and green bundles. Since most of the actin bundles eventually adhered to surfaces, it was not possible to observe extended time evolution *in situ*. Instead, fresh slides were prepared from an evolving sample at different times.

The distribution of red and green filaments within a bundle depends sensitively on the initial $[Mg^{2+}]$ prior to mixing of red and green bundles. On the first row of Fig. 2, different ensembles of red and green bundles are shown for 30, 50, and 100 mM $MgCl_2$ after initial mixing. The background of uncondensed red and green *F*-actin filaments is clearly visible for the 30 mM sample

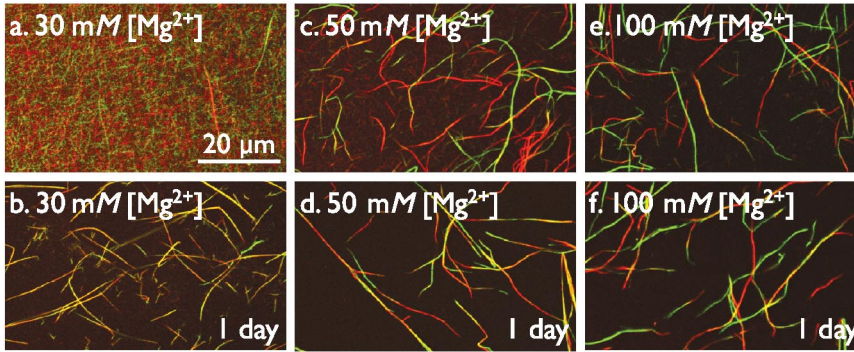


FIG. 2 (color). Filament population mixing within bundles initially and after ~ 30 h at 30 mM, 50 mM and 100 mM $[\text{Mg}^{2+}]$. The significant background of red and green filaments at low salt fades away with increasing salt and time. Occurrence of yellow regions decreases as we increase initial $[\text{Mg}^{2+}]$.

[Fig. 2(a)], with few green and red bundles formed. Upon increasing $[\text{Mg}^{2+}]$, we observe more bundle formation (and less of the uncondensed F -actin background). For all $[\text{Mg}^{2+}]$, few junctions are observed between red and green bundles initially. We see a significant increase in frequency of junctions after 1 h. Bundle junction formation falls off drastically after a day, with samples shown in the second row of Fig. 2. For the 30 mM salt sample, the bundles are already predominantly yellow after an hour, indicating a mixed population of red and green filaments. With higher initial salt concentration, short segments of pure green and pure red appear between long yellow junctions. The fraction of pure red and green segments becomes larger with increasing salt until bundles are organized into distinct red and green segments with relatively abrupt red-green junctions.

Possible mechanisms for this long-term behavior include salt-dependent mobility and mixing within a bundle, and salt-dependent availability of free filaments in solution. The first hypothesis implies high filament mobility within a bundle at low salt. We conducted fluorescence recovery after photobleaching (FRAP) experiments by bleaching micron-sized spots on single-colored actin bundles in low salt and observed no recovery within 2 h, so the longitudinal mobility of filaments within bundles is limited. Although sliding is likely important for the initial stages of bundle formation [16,22], this suggests that when filaments get added to mature, preformed bundles at the bundle lengthening stage of growth, they do not slide appreciably along the bundles, and are analogous to diffusion-limited aggregation clusters of sticky colloids.

In the second hypothesis, the salt concentration controls the availability of single filaments in solution, which grow from the ends of existing bundles that eventually aggregate together longitudinally. This implies long yellow junctions for low salt, where there is significant concentration of free filaments to add to existing bundles, and little or no yellow junctions for high salt, where free filaments are depleted, in agreement with observations. To test this, two week-old separate populations of 30 mM $[\text{Mg}^{2+}]$ red and green bundles (with presumably depleted free filaments) were mixed. Distinct red and green bundles were observed after an hour with very few junctions, all of which consist of red and green bundle segments with no yellow mixed junc-

tions, in sharp contrast with earlier results of yellow bundles [Fig. 2(b)]. Moreover, we used 2-month-old equilibrated red bundles that were no longer evolving, and added fresh trace amounts of green filaments. New longitudinal junctions were again observed in this case, in support of the salt-dependent filament availability hypothesis. Because of entropy, all bundles should evolve towards a completely mixed state, or a uniform yellow color in the long equilibration time limit. The fact that this is not observed, and that “aged” bundles do not converge with those of Fig. 2 are consistent with the low longitudinal filament mobility within the bundles from FRAP measurements [23].

We quantitatively characterize how filaments add to bundles by monitoring the time evolution of bundle junction densities. The frequency of bundle junctions (yellow domains) has a fast initial increase upon mixing, followed by a progressively slower evolution which we focus on to access the long-time growth behavior of mature bundles (Fig. 3). When the red and green bundle-filament-salt solutions are mixed, the available filaments will undergo a “floculation” process whose kinetics is diffusion-limited because of their low density. We model this process by using the Smoluchowski cluster size distribution during floculation [24]. The density of clusters with k filaments will have a form $n_k(t) = \frac{n_0(t/t_p)^{k-1}}{(1+t/t_p)^{k+1}}$, where n_0

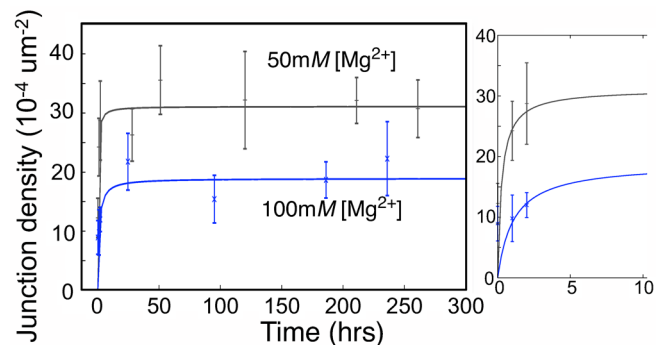


FIG. 3 (color online). Evolution of observable junction density n_{2d} , with fitting function $n_{2d} = n_{2d}^0 \frac{t}{t+t_p}$, at 50 mM and 100 mM $[\text{Mg}^{2+}]$. Right subplot shows the initial rapid growth with time. $n_{2d}^0 = 31.1 \pm 3.6 \times 10^{-4} \mu\text{m}^{-2}$, $t_p = 0.3 \pm 0.4$ h for 50 mM $[\text{Mg}^{2+}]$ and $n_{2d}^0 = 18.9 \pm 3.3 \times 10^{-4} \mu\text{m}^{-2}$, $t_p = 1.1 \pm 0.9$ h for 100 mM $[\text{Mg}^{2+}]$.

is the initial concentration of available filaments and $t_p = (\eta W)/(n_0 k_B T)$ (within a numerical prefactor), where η is the viscosity (water) and $W = \exp(\Delta E_a/k_B T)$ with ΔE_a as the activation barrier. The yellow actin patches comprise all of the actin filaments (not bundles) we had in the beginning minus the present actin density in the form of single filaments, doublets, triplets, and so on, whose density can be calculated as $\sum_{k=1}^{\infty} \frac{n_0(t/t_p)^{k-1}}{(1+t/t_p)^{k+1}} = \frac{n_0}{(1+t/t_p)}$. The filament density consumed in junctions is then $\sim n_0(\frac{t}{1+t_p})$. A recent computer simulation confirms that this is a feasible description of bundle formation kinetics [16].

The saturation behavior of this slowest mode of bundle growth imposes strong quantitative constraints on the kinetics governing the system. Junctions were measured by averaging at least 15 images ($\sim 120 \mu\text{m} \times 120 \mu\text{m}$) per data point. While we do not have experimental access to short times with confocal microscopy, the junction density data clearly show asymptotic plateaus for the limiting long-time behavior, from which we estimate ΔE_a using the fitted 2D junction density (Fig. 3). Experimentally, essentially all the bundles lie in either the cover slip plane or the plane of the slide, therefore we estimate the equilibrium 2D junction density via the integral of the volume density over the vertical span D ($\sim 17 \mu\text{m}$ between slide and cover slip) through $n_{3d}D \approx 2n_{2d}^0$. Furthermore, if all the F -actin is consumed by junction formation, then $n_0 \approx n_{3d}\sigma$, where σ parametrizes the average number of filaments consumed at each junction. The measured saturation bundle width suggests ~ 30 F -actin rods per bundle for perfect packing, and significantly less if defects are present, as suggested by x-ray data [4]. With this limit on σ , we estimate ΔE_a to range from 2.3 – $3.1k_B T$ ($\sigma = 10$) to 3.4 – $4.2k_B T$ ($\sigma = 30$) at 5°C . These are relatively small values for the activation barrier of filament addition at the final stages of bundle growth, which in fact saturates much more slowly than initial lateral growth. It is therefore unlikely that observed finite bundle widths are significantly limited by kinetics.

We thank B.H. Lee and M. Shim for the ZnS/CdSe quantum dots, and J.C. Conrad and J.A. Lewis for their suggestions. This material is based upon work supported by the U.S. Department of Energy (No. DEFG02-91ER45439) through the Frederick Seitz Materials Research Laboratory.

*Email address: gclwong@uiuc.edu

- [1] *Electrostatic Effects in Soft Matter and Biophysics*, NATO Advanced Science Series II Vol. 46, edited by C. Holm, P. Kekicheff, and R. Podgornik (Kluwer, Dordrecht, 2001); Y. Levin, Rep. Prog. Phys. **65**, 1577 (2002).
- [2] R. Podgornik, D. C. Rau, and V. A. Parsegian, Biophys. J. **66**, 962 (1994); V. A. Bloomfield, Curr. Opin. Struct. Biol. **6**, 334 (1996); J. X. Tang and P. A. Janmey, J. Biol. Chem. **271**, 8556 (1996); J. X. Tang, T. Ito, T. Tao, P. Traub, and P. A. Janmey, Biochemistry **36**, 12600 (1997); A. P. Lyubartsev, J. X. Tang, P. A. Janmey, and L. Nordenskiöld, Phys. Rev. Lett. **81**, 5465 (1998).
- [3] V. A. Bloomfield, Biopolymers **31**, 1471 (1991).
- [4] T. E. Angelini, H. Liang, W. Wriggers, and G. C. L. Wong, Proc. Natl. Acad. Sci. U.S.A. **100**, 8634 (2003).
- [5] J. C. Butler, T. Angelini, J. X. Tang, and G. C. L. Wong, Phys. Rev. Lett. **91**, 028301 (2003).
- [6] D. J. Needleman, M. A. Ojeda-Lopez, U. Raviv, H. P. Miller, L. Wilson, and C. R. Safinya, Proc. Natl. Acad. Sci. U.S.A. **101**, 16099 (2004).
- [7] J. Widom and R. L. Baldwin, Biopolymers **22**, 1595 (1983).
- [8] G. C. L. Wong, A. Lin, J. X. Tang, Y. Li, P. A. Janmey, and C. R. Safinya, Phys. Rev. Lett. **91**, 018103 (2003); I. Borukhov, R. F. Bruinsma, W. M. Gelbart, and A. J. Liu, Proc. Natl. Acad. Sci. U.S.A. **102**, 3673 (2005).
- [9] D. J. Weiner, R. Bucki, and P. A. Janmey, Am. J. Respir. Cell Mol. Biol. **28**, 738 (2003); L. K. Sanders, C. Guáqueta, T. E. Angelini, J.-W. Lee, S. C. Slimmer, E. Luijten, and G. C. L. Wong, Phys. Rev. Lett. **95**, 108302 (2005).
- [10] O. V. Zribi, H. Kyung, R. Golestanian, T. B. Liverpool, and G. C. L. Wong, Europhys. Lett. **70**, 541 (2005).
- [11] B.-Y. Ha and A. J. Liu, Phys. Rev. Lett. **81**, 1011 (1998); B. I. Shklovskii, Phys. Rev. Lett. **82**, 3268 (1999); C.-I. Huang and M. Olvera de la Cruz, Macromolecules **35**, 976 (2002).
- [12] B.-Y. Ha and A. J. Liu, Europhys. Lett. **46**, 624 (1999).
- [13] M. L. Henle and P. A. Pincus, Phys. Rev. E **71**, 060801(R) (2005).
- [14] M. J. Stevens, Phys. Rev. Lett. **82**, 101 (1999).
- [15] H. J. Limbach, M. Sayar, and C. Holm, J. Phys. Condens. Matter **16**, S2135 (2004).
- [16] H. Fazli and R. Golestanian (unpublished).
- [17] M. A. Bevan, J. A. Lewis, P. V. Braun, and P. Wiltzius, Langmuir **20**, 7045 (2004).
- [18] See EPAPS Document No. E-PRLTAO-98-060715 for supplementary animation, using techniques from [17], which can be reached via a direct link in the online article's HTML reference section or via the EPAPS homepage. For more information on EPAPS, see <http://www.aip.org/pubservs/epaps.html>.
- [19] Since red bundles can join with other red bundles, the lack of an observable longitudinal red-green junction is not sufficient proof that no junction has occurred.
- [20] Candidates for lateral growth were observed at low salt, but they are rare (1 candidate in 20 junctions) compared to the dominant longitudinal growth.
- [21] J. Hanson, Proc. R. Soc. B **183**, 39 (1973).
- [22] I. Borukhov, K.-C. Lee, R. F. Bruinsma, W. M. Gelbart, A. J. Liu, and M. J. Stevens, J. Chem. Phys. **117**, 462 (2002).
- [23] In the limit that the green and red labels do not alter the interactions between filaments, then a bundle's internal color distribution does not denote distinct structural arrangements.
- [24] W. B. Russel, D. A. Saville, and W. R. Schowalter, *Colloidal Dispersions* (Cambridge University Press, Cambridge, U.K., 1988).